FAST HUYGENS SWEEPING METHODS FOR TIME-DEPENDENT SCHRÖDINGER EQUATION WITH PERFECTLY MATCHED LAYERS*

SONGTING LUO[†]

Abstract. We present asymptotic methods for numerically solving the time-dependent Schrödinger equation with time-dependent potentials. The methods consist of the following ingredients: (1) perfectly matched layers are applied to limit the infinite domain to a bounded subdomain; (2) the wavefunction is propagated by a short-time propagator in the form of integrals with retarded Green's functions that are based on Huygens' principle; (3) semiclassical limit approximations are adopted to approximate the retarded Green's functions, where the phase and amplitude terms are obtained as solutions of eikonal and transport equations, respectively; (4) Taylor expansions are explored to obtain analytic approximations of the phase and amplitude terms for a short period of time; and (5) the fast Fourier transform can be used to evaluate the integrals after appropriate low-rank approximations with Chebyshev polynomial interpolation. The methods are expected to have complexity $O(N \log N)$ per time step with N the number of points used in the simulation. Numerical examples are presented to demonstrate the methods.

Key words. Schrödinger equation, fast Huygens sweeping, low-rank approximations, Chebyshev interpolation, fast Fourier transform

AMS subject classifications. 65M80, 41A60

DOI. 10.1137/18M119690X

1. Introduction. We consider numerical methods for solving the time-dependent Schrödinger equation:

(1.1)
$$\iota\hbar \frac{\partial \phi(\mathbf{x}, t)}{\partial t} = -\frac{\hbar^2}{2m} \nabla^2 \phi(\mathbf{x}, t) + v(\mathbf{x}, t) \phi(\mathbf{x}, t), \ t > 0,$$
$$\phi(\mathbf{x}, 0) = \phi_0(\mathbf{x}),$$

where $\mathbf{x} \equiv (x, y, z) \in \mathbf{R}^3$ is the spatial coordinate vector, $\nabla \equiv (\partial_x, \partial_y, \partial_z)$ is the gradient operator at \mathbf{x} , m is the atomic mass, \hbar is the reduced Planck constant, $\phi(\mathbf{x}, t)$ is the wavefunction, $v(\mathbf{x}, t)$ is the time-dependent potential, and $\phi_0(\mathbf{x})$ is the initial wavefunction. Numerical solutions of the Schrödinger equation (1.1) are desirable for its wide applications in engineering, physics, and chemistry. However, solving the equation numerically is highly challenging, mainly because (i) the domain is infinite, and (ii) the wavefunction ϕ is oscillatory for small parameter \hbar .

For computing the wavefunction in an infinite domain, unless the wavefunction is assumed to be compactly supported in a bounded subdomain, the aim is to compute the wavefunction around a small bounded subdomain that bears special physical interest. A common practice of accomplishing such a goal is to "truncate" the computational domain and solve a "truncated" problem with a suitable domain-based method, where absorbing boundary conditions (ABCs) are generally required. As one of the approaches for designing ABCs, the perfectly matched layer (PML) method

Funding: This work was partially funded by NSF DMS 1418908 and 1719907.

^{*}Submitted to the journal's Methods and Algorithms for Scientific Computing section June 27, 2018; accepted for publication (in revised form) February 14, 2019; published electronically March 26, 2019.

 $[\]rm http://www.siam.org/journals/sisc/41-2/M119690.html$

[†]Department of Mathematics, Iowa State University, Ames, IA, 50011 (luos@iastate.edu).

has achieved great success in various applications. The perfectly matched layer, ever since it was introduced by Berenger in 1994 [9], has become a widespread technique for preventing reflections from far field boundaries for wave propagation problems in both the time-dependent and frequency domains. The idea is to use an absorbing layer designed to absorb waves without reflections. The PML can be seen as the result of a complex coordinate transformation, being essentially a continuation of the equation into complex spatial coordinates, where a modified equation has to be solved. Ideally, the incoming waves are damped to such an extent that the outer boundary conditions are of no importance. Also, the interface between the computational domain and the damping layer should not cause any reflections. In our numerical simulation, we will first use the PML method to "truncate" the infinite domain to a bounded subdomain and derive the modified equation in the bounded subdomain.

The wavefunction ϕ is highly oscillatory for small parameter \hbar such that it is very challenging to compute if methods based on direct discretization of the equation, such as the finite difference and finite element methods, are used. Because in order to control the dispersion error, such methods require very refined meshes to resolve the oscillations, and their computational cost becomes too high for practical applications [3, 4, 16]. Therefore, alternative methods such as the operator splitting methods and the asymptotic methods in the semiclassical regime [2, 6, 7, 8, 19, 22, 30] have been designed to balance efficiency and accuracy. In our numerical simulation, we propose to design asymptotic methods in the semiclassical regime by approximating the time propagator of the wavefunction ϕ in a way that combines Huygens' principle [5] and the Wentzel-Kramers-Brillouin-Jeffreys (WKBJ) propagator [10, 13, 20, 22, 25, 26].

The time propagator of the wavefunction ϕ can be given as integrals with the retarded Green's functions [29, 31]. The retarded Green's function for a generic source (\mathbf{x}_0, t_0) , denoted as $G(\mathbf{x}, t; \mathbf{x}_0, t_0)$, satisfies the equation:

(1.2)
$$\iota\hbar \frac{\partial G(\mathbf{x}, t; \mathbf{x}_0, t_0)}{\partial t} = -\frac{\hbar^2}{2m} \nabla^2 G(\mathbf{x}, t; \mathbf{x}_0, t_0) + v(\mathbf{x}, t) G(\mathbf{x}, t; \mathbf{x}_0, t_0), \ t > t_0,$$
$$\lim_{t \to t_0^+} G(\mathbf{x}, t; \mathbf{x}_0, t_0) = \delta(\mathbf{x} - \mathbf{x}_0),$$
$$G(\mathbf{x}, t; \mathbf{x}_0, t_0) = 0, \ t < t_0.$$

According to Huygens' principle [29, 31], the wavefunction $\phi(\mathbf{x}, t)$ for $t > t_0$ is given as

(1.3)
$$\phi(\mathbf{x},t) = \int_{\mathbf{R}^3} G(\mathbf{x},t;\mathbf{x}_0,t_0)\phi(\mathbf{x}_0,t_0)d\mathbf{x}_0, \ t > t_0.$$

In order to apply the above integral for computing the wavefunction ϕ , the retarded Green's function G must be computed and it requires solving (1.2), which can be as challenging as solving (1.1). Instead, we turn to seek asymptotic approximations with the WKBJ ansatz [16, 20, 25, 26]:

(1.4)
$$\tilde{G}(\mathbf{x}, t; t_0; \boldsymbol{\xi}) = \exp(\iota \tau(\mathbf{x}, t; t_0; \boldsymbol{\xi}) / \hbar) A(\mathbf{x}, t; t_0; \boldsymbol{\xi}; \hbar) \\
\equiv \exp(\iota \tau(\mathbf{x}, t; t_0; \boldsymbol{\xi}) / \hbar) \left\{ \sum_{k=0}^{\infty} (-\iota \hbar)^k A_k(\mathbf{x}, t; t_0; \boldsymbol{\xi}) \right\},$$

as $\hbar \to 0$ for any given parameter $\boldsymbol{\xi} \in \mathbf{R}^3$, where τ is the phase and $\{A_k\}_{k=0}^{\infty}$ are the amplitude terms, and \tilde{G} satisfies the following equation in the semiclassical limit:

(1.5)
$$\iota\hbar \frac{\partial \tilde{G}(\mathbf{x}, t; t_0; \boldsymbol{\xi})}{\partial t} = -\frac{\hbar^2}{2m} \nabla^2 \tilde{G}(\mathbf{x}, t; t_0; \boldsymbol{\xi}) + v(\mathbf{x}, t) \tilde{G}(\mathbf{x}, t; t_0; \boldsymbol{\xi}), \ t > t_0,$$
$$\tilde{G}(\mathbf{x}, t_0; t_0; \boldsymbol{\xi}) = \exp(\iota \mathbf{x} \cdot \boldsymbol{\xi}).$$

By substituting (1.4) into (1.5) and collecting terms in the same order of \hbar as $\hbar \to 0$, for each parameter ξ , one can derive the eikonal equation for $\tau(\mathbf{x}, t; t_0; \boldsymbol{\xi})$,

(1.6)
$$\tau_t + v(\mathbf{x}, t) + \frac{1}{2m} |\nabla \tau|^2 = 0, \ t > t_0,$$
$$\tau(\mathbf{x}, t_0; t_0; \boldsymbol{\xi}) = \mathbf{x} \cdot \boldsymbol{\xi},$$

and the transport equations for $\{A_k(\mathbf{x},t;t_0;\boldsymbol{\xi})\}_{k=0}^{\infty}$,

(1.7)
$$(A_0)_t + \frac{1}{m} \nabla \tau \cdot \nabla A_0 + \frac{1}{2m} \Delta \tau A_0 = 0, \ t > t_0,$$

$$A_0(\mathbf{x}, t_0; \boldsymbol{\xi}) = 1,$$

and for $k \geq 1$,

(1.8)
$$(A_k)_t + \frac{1}{m} \nabla \tau \cdot \nabla A_k + \frac{1}{2m} \Delta \tau A_k = -\frac{\Delta A_{k-1}}{2m}, \ t > t_0,$$

$$A_k(\mathbf{x}, t_0; t_0; \boldsymbol{\xi}) = 0.$$

With the plane wave decomposition of the δ -function given as

$$\delta(\mathbf{x} - \mathbf{x}_0) = \left(\frac{1}{2\pi\hbar}\right)^3 \int_{\mathbf{R}^3} \exp(\iota(\mathbf{x} \cdot \boldsymbol{\xi} - \mathbf{x}_0 \cdot \boldsymbol{\xi})/\hbar) d\boldsymbol{\xi},$$

one can approximate the retarded Green's function as

(1.9)

$$G(\mathbf{x}, t; \mathbf{x}_0, t_0) = \left(\frac{1}{2\pi\hbar}\right)^3 \int_{\mathbf{R}^3} \exp(\iota(\tau(\mathbf{x}, t; t_0; \boldsymbol{\xi}) - \mathbf{x}_0 \cdot \boldsymbol{\xi})/\hbar) \sum_{k=0}^{\infty} A_k(\mathbf{x}, t; t_0; \boldsymbol{\xi}) (-\iota\hbar)^k d\boldsymbol{\xi},$$

for a short period of time, $t \in [t_0, t_0 + \Delta t]$ with Δt small, while the phase τ and the amplitude terms $\{A_k\}_{k=0}^{\infty}$ are smooth [22].

With the asymptotic retarded Green's function (1.9), the wavefunction ϕ can be propagated for a short period of time starting from any arbitrary time t_0 [18, 21, 22]:

(1.10)
$$\phi(\mathbf{x},t) = \int_{\mathbf{R}^3} G(\mathbf{x},t;\mathbf{x}_0,t_0)\phi(\mathbf{x}_0,t_0)d\mathbf{x}_0, \ t_0 < t < t_0 + \Delta t.$$

The local short-time propagation can be repeated to propagate the wavefunction ϕ for a long time [18, 21]:

(1.11)
$$\phi(\mathbf{x},t) = \int_{\mathbf{R}^3} G(\mathbf{x},t;\mathbf{x}_0,t_k)\phi(\mathbf{x}_0,t_k)d\mathbf{x}_0, \ t_k < t < t_k + \Delta t,$$

with $t_k = k\Delta t$ for $k = 0, 1, 2, \dots$

The short-time propagator that combines Huygens' principle and the WKBJ ansatz has been applied to compute semiclassical solutions of the Schrödinger equations with time-independent potentials [22], where the solutions are assumed to be compactly supported such that the computation can be performed in a bounded subdomain. Analytic approximations of the phase and amplitude terms within a short period of time are obtained by Taylor expansions. And the integral (1.10) can be

evaluated by the fast Fourier transform (FFT) after appropriate discretization. Consequently, the overall complexity at each time step is $O(N \log N)$ with N the number of points used in the simulation. Similar techniques that combine integral representations of the wavefunction and asymptotic approximations of the Green's functions have been developed for simulating acoustic and electromagnetic wave propagation in the high frequency regime [23, 27, 28]. These methods are based on Huygens' principle, and their complexity is $O(N \log N)$ because the integrals can be evaluated efficiently via low-rank approximations of the matrix obtained from discretizing the integrals.

In this work, we extend the ideas to compute asymptotic solutions for the Schrödinger equation with time-dependent potentials (1.1) and PMLs. The PML method is first applied to limit the infinite domain to a bounded subdomain without assuming that the wavefunction is compactly supported. After that, we derive the modified Schrödinger equation with the PMLs in the "truncated" subdomain, following which we present asymptotic approximations of the short-time propagator for its wavefunction by combining Huygens' principle and the WKBJ approximation. With the asymptotic approximations of the short-time propagator, we propose efficient numerical procedures to evaluate the integrals. Appropriate low-rank approximations with Chebyshev polynomial interpolation will be applied to approximate the integrals such that the resulting integrals can be evaluated by the FFT. Therefore, we can compute globally asymptotic solutions for the Schrödinger equation efficiently.

The rest of the paper is organized as follows. In section 2, we first present the modified Schrödinger equation with the PMLs and asymptotic approximations of the short-time propagator for its wavefunction; then we show how to approximate the phase τ and amplitude terms $\{A_k\}_{k=0}^{\infty}$ analytically in the asymptotic approximation, and finally we present the formulations and numerical procedures for computing the wavefunction efficiently. In section 3, we demonstrate the methods with numerical experiments, including time-dependent Gross-Pitaevskii equations for Bose-Einstein condensation at zero temperature. Conclusive remarks are given at the end.

2. Formulations and algorithms. In this section, we present asymptotic methods for the Schrödinger equation with perfectly matched layers. We assume the computational domain is $\Omega = [x_{\min}, x_{\max}] \times [y_{\min}, y_{\max}] \times [z_{\min}, z_{\max}]$, which is covered by a uniform mesh $\{\mathbf{x}_{iijjkk} \equiv (x_{ii}, y_{jj}, z_{kk})\}$ as

$$\{x_{ii} \equiv x_{\min} + (ii - 1)\Delta x\}_{ii=1}^{N_x + 1},$$

$$\{y_{jj} \equiv y_{\min} + (jj - 1)\Delta y\}_{jj=1}^{N_y + 1},$$

$$\{z_{kk} \equiv z_{\min} + (kk - 1)\Delta z\}_{kk=1}^{N_z + 1},$$

with $\Delta x = (x_{\text{max}} - x_{\text{min}})/N_x$, $\Delta y = (y_{\text{max}} - y_{\text{min}})/N_y$, $\Delta z = (z_{\text{max}} - z_{\text{min}})/N_z$. We also assume the phase domain $\boldsymbol{\xi} \equiv (\xi_1, \xi_2, \xi_3)$ is covered by a uniform mesh $\{\boldsymbol{\xi}_{ijk} \equiv (\xi_{1i}, \xi_{2j}, \xi_{3k})\}$ as

$$\begin{split} & \left\{ \xi_{1i} \equiv (i-1) \Delta \xi_1 \right\}_{i=-N_x/2+1}^{N_x/2}, \\ & \left\{ \xi_{2j} \equiv (j-1) \Delta \xi_2 \right\}_{j=-N_y/2+1}^{N_y/2}, \\ & \left\{ \xi_{3k} \equiv (k-1) \Delta \xi_3 \right\}_{k=-N_z/2+1}^{N_z/2}, \end{split}$$

with $\Delta \xi_1 = 2\pi/(x_{\text{max}} - x_{\text{min}})$, $\Delta \xi_2 = 2\pi/(y_{\text{max}} - y_{\text{min}})$, $\Delta \xi_3 = 2\pi/(z_{\text{max}} - z_{\text{min}})$.

2.1. Schrödinger equation with PML. We shall derive the Schrödinger equation with the PMLs using the complex coordinate stretching technique. Introduce the absorption profile functions [1, 9, 32]:

(2.1)
$$\sigma(l) = \begin{cases} C_l \left| \frac{l - l_{\min} - \eta_l}{\eta_l} \right|^p, & l \in [l_{\min}, \ l_{\min} + \eta_l], \\ 0, & l \in [l_{\min}, \ l_{\max} - \eta_l], \\ C_l \left| \frac{l - l_{\max} + \eta_l}{\eta_l} \right|^p, & l \in [l_{\max} - \eta_l, \ l_{\max}], \end{cases}$$

and

$$s(l) = \frac{1}{1 + \exp(i\pi/4)\sigma(l)}$$

Here $[l_{\min}, l_{\max}]$ is the interval of interest, η_l is the width of the PML, C_l is constant, and p is the power of the profile function. The PML method replaces ∂_x, ∂_y , and ∂_z with $s_1(x)\partial_x, s_2(y)\partial_y$, and $s_3(z)\partial_z$, respectively, where $s_i(\cdot) = s(\cdot)$ with $\sigma_i(\cdot) = \sigma(\cdot)$ for i = 1, 2, 3. The PML effectively provides a damping layer of width η_x (η_y, η_z , respectively) near the two sides of the x-axis (y-axis, z-axis, respectively); refer to Figure 1.

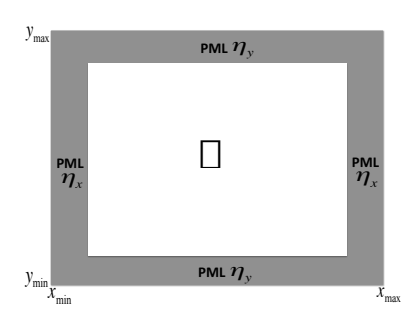


Fig. 1. PML for two-dimensional cases: with width η_x and η_y along the x-axis and y-axis, respectively.

The Schrödinger equation (1.1) transfers to

$$\iota\hbar\frac{\partial\phi(\mathbf{x},t)}{\partial t} = -\frac{\hbar^2}{2m}\{s_1(x)\partial_x(s_1(x)\partial_x) + s_2(y)\partial_y(s_2(y)\partial_y) + s_3(z)\partial_z(s_3(z)\partial_z)\}\phi(\mathbf{x},t) + v(\mathbf{x},t)\phi(\mathbf{x},t).$$

By substituting $\phi(\mathbf{x},t)$ with

$$\phi(\mathbf{x},t) = \frac{\psi(\mathbf{x},t)}{\sqrt{s_1(x)s_2(y)s_3(z)}},$$

we have the modified Schrödinger equation:

(2.2)
$$\iota\hbar \frac{\partial \psi(\mathbf{x},t)}{\partial t} = -\frac{\hbar^2}{2m_1(x)} \psi_{xx}(\mathbf{x},t) - \frac{\hbar^2}{2m_2(y)} \psi_{yy}(\mathbf{x},t) - \frac{\hbar^2}{2m_3(z)} \psi_{zz}(\mathbf{x},t) + w(\mathbf{x},t)\psi(\mathbf{x},t),$$
with
$$m_1(x) = \frac{m}{s_1^2(x)}, \ m_2(y) = \frac{m}{s_2^2(y)}, \ m_3(z) = \frac{m}{s_3^2(z)},$$

and

$$\begin{split} & w(\mathbf{x},t) \\ & = -\frac{\hbar^2}{2m} \left(\!\! \frac{(s_1'(x))^2 + (s_2'(y))^2 + (s_3'(z))^2}{4} - \frac{s_1(x)s_1''(x) + s_2(y)s_2''(y) + s_3(z)s_3''(z)}{2} \!\! \right) + v(\mathbf{x},t). \end{split}$$

The time propagator of the wavefunction ψ is also given as integrals with the retarded Green's functions [29, 31], similarly as in the introduction (section 1). The retarded Green's function for a generic source (\mathbf{x}_0, t_0) , also denoted as $G(\mathbf{x}, t; \mathbf{x}_0, t_0)$, satisfies the equation:

$$\iota\hbar \frac{\partial G}{\partial t} = -\frac{\hbar^2}{2m_1(x)} G_{xx} - \frac{\hbar^2}{2m_2(y)} G_{yy} - \frac{\hbar^2}{2m_3(z)} G_{zz} + wG, \ t > t_0,$$
(2.3)
$$\lim_{t \to t_0^+} G(\mathbf{x}, t; \mathbf{x}_0, t_0) = \delta(\mathbf{x} - \mathbf{x}_0),$$

$$G(\mathbf{x}, t; \mathbf{x}_0, t_0) = 0, \ t < t_0.$$

Following Huygens' principle [29, 31], the wavefunction $\psi(\mathbf{x},t)$ for $t > t_0$ is given as

(2.4)
$$\psi(\mathbf{x},t) = \int_{\Omega} G(\mathbf{x},t;\mathbf{x}_0,t_0)\psi(\mathbf{x}_0,t_0)d\mathbf{x}_0, \ t > t_0.$$

2.2. Asymptotic approximation. We explore asymptotic approximations of the retarded Green's function G with the WKBJ ansatz (1.4) and choose $\tilde{G}(\mathbf{x},t;t_0;\boldsymbol{\xi})$ that satisfies the following equation:

(2.5)
$$\iota\hbar\frac{\partial\tilde{G}}{\partial t} = -\frac{\hbar^2}{2m_1(x)}\tilde{G}_{xx} - \frac{\hbar^2}{2m_2(y)}\tilde{G}_{yy} - \frac{\hbar^2}{2m_3(z)}\tilde{G}_{zz} + w\tilde{G}, \ t > t_0,$$
$$\tilde{G}(\mathbf{x}, t_0; t_0; \boldsymbol{\xi}) = \exp(\iota\mathbf{x} \cdot \boldsymbol{\xi}).$$

With formulas (1.9) and (2.4), one can derive the approximation of ψ as

$$\psi(\mathbf{x},t) = \int_{\Omega} G(\mathbf{x},t;\mathbf{x}_{0},t_{0})\psi(\mathbf{x}_{0},t_{0})d\mathbf{x}_{0}$$

$$= \left(\frac{1}{2\pi\hbar}\right)^{3} \int_{\Omega} \int_{\mathbf{R}^{3}} \exp(\iota(\tau(\mathbf{x},t;t_{0};\boldsymbol{\xi})-x_{0}\cdot\boldsymbol{\xi})/\hbar)$$

$$\times \sum_{k=0}^{\infty} A_{k}(\mathbf{x},t;t_{0};\boldsymbol{\xi})(-\iota\hbar)^{k}\psi(\mathbf{x}_{0},t_{0})d\boldsymbol{\xi}d\mathbf{x}_{0}$$

$$= \sum_{k=0}^{\infty} \int_{\mathbf{R}^{3}} \exp(\iota\tau(\mathbf{x},t;t_{0};\boldsymbol{\xi})/\hbar)A_{k}(\mathbf{x},t;t_{0};\boldsymbol{\xi})(-\iota\hbar)^{k}\hat{\psi}(\boldsymbol{\xi},t_{0})d\boldsymbol{\xi},$$

with $\hat{\psi} \equiv \mathcal{F}[\psi]$ the Fourier transform of ψ :

(2.7)
$$\hat{\psi}(\boldsymbol{\xi}, t_0) \equiv \mathcal{F}[\psi(\mathbf{x}, t_0)] = \left(\frac{1}{2\pi\hbar}\right)^3 \int_{\Omega} \exp(-\iota \mathbf{x}_0 \cdot \boldsymbol{\xi}/\hbar) \psi(\mathbf{x}_0, t_0) d\mathbf{x}_0.$$

Formula (2.6) will serve as the short-time propagator for the wavefunction ψ . For numerical implementations, we need to truncate the infinite sum and compute the phase and amplitude terms needed in the truncated sum.

2.3. Analytic approximations of phase and amplitude terms. The modified eikonal equation for $\tau(\mathbf{x}, t; t_0; \boldsymbol{\xi})$ is given as

(2.8)
$$\frac{\partial \tau}{\partial t} + \frac{\tau_x^2}{2m_1(x)} + \frac{\tau_y^2}{2m_2(y)} + \frac{\tau_z^2}{2m_3(z)} + w(\mathbf{x}, t) = 0, \ t > t_0,$$
$$\tau(\mathbf{x}, t_0; \boldsymbol{t}_0; \boldsymbol{\xi}) = \mathbf{x} \cdot \boldsymbol{\xi},$$

and the modified transport equations for $\{A_k(\mathbf{x},t;t_0;\boldsymbol{\xi})\}_{k=0}^{\infty}$ are given as

(2.9)
$$(A_0)_t + \frac{(A_0)_x \tau_x}{m_1(x)} + \frac{(A_0)_y \tau_y}{m_2(y)} + \frac{(A_0)_z \tau_z}{m_3(z)}$$

$$+ \left(\frac{\tau_{xx}}{2m_1(x)} + \frac{\tau_{yy}}{2m_2(y)} + \frac{\tau_{zz}}{2m_3(z)}\right) A_0 = 0, \ t > t_0,$$

$$A_0(\mathbf{x}, t_0; t_0; \boldsymbol{\xi}) = 1,$$

and for k > 1,

(2.10)

$$(A_k)_t + \frac{(A_k)_x \tau_x}{m_1(x)} + \frac{(A_k)_y \tau_y}{m_2(y)} + \frac{(A_k)_z \tau_z}{m_3(z)} + \left(\frac{\tau_{xx}}{2m_1(x)} + \frac{\tau_{yy}}{2m_2(y)} + \frac{\tau_{zz}}{2m_3(z)}\right) A_k$$

$$= -\frac{(A_{k-1})_{xx}}{2m_1(x)} - \frac{(A_{k-1})_{yy}}{2m_2(y)} - \frac{(A_{k-1})_{zz}}{2m_3(z)}, \ t > t_0,$$

$$A_k(\mathbf{x}, t_0; t_0; \boldsymbol{\xi}) = 0.$$

The computation of τ and $\{A_k\}_{k=0}^{\infty}$ is the most expensive part for implementing (2.6), since they must be computed for all $\boldsymbol{\xi} \in \mathbf{R}^3$. To alleviate the computational burden, we follow the approaches in [17, 22, 24], where analytic approximations of τ and $\{A_k\}_{k=0}^{\infty}$ are obtained with short-time Taylor expansions.

Assume that we need to approximate $\tau(\mathbf{x}, t; t_0; \boldsymbol{\xi})$ and $\{A_k(\mathbf{x}, t; t_0; \boldsymbol{\xi})\}_{k=0}^{\infty}$ at $t = t_0 + \Delta t$ with Δt small. We expand them as Taylor series at t_0 :

(2.11)
$$\tau(\mathbf{x}, t; t_0; \boldsymbol{\xi}) = \sum_{l=0}^{\infty} \tau_l(\mathbf{x}; t_0; \boldsymbol{\xi}) (\Delta t)^l,$$
$$A_k(\mathbf{x}, t; t_0; \boldsymbol{\xi}) = \sum_{l=0}^{\infty} A_{kl}(\mathbf{x}; t_0; \boldsymbol{\xi}) (\Delta t)^l, \ k \ge 0,$$

with the expansion terms, $\{\tau_l\}_{l=0}^{\infty}$ and $\{A_{kl}\}_{l=0}^{\infty}$, to be determined. And we assume the Taylor series for $w(\mathbf{x},t)$ at t_0 is given:

$$w(\mathbf{x},t) = \sum_{l=0}^{\infty} w_l(\mathbf{x},t_0) \Delta t^l \equiv \sum_{l=0}^{\infty} \left\{ \frac{1}{l!} \frac{\partial^l w(\mathbf{x},t_0)}{\partial t^l} \right\} \Delta t^l.$$

By substituting the Taylor series for τ into the eikonal equation (2.8) and collecting the terms of the same order in Δt , we have

$$\tau_0(\mathbf{x}; t_0; \boldsymbol{\xi}) = \mathbf{x} \cdot \boldsymbol{\xi},$$

$$\tau_{1}(\mathbf{x}; t_{0}; \boldsymbol{\xi}) = -\frac{\boldsymbol{\xi}^{2}}{2} \cdot \left(\frac{1}{m_{1}(x)}, \frac{1}{m_{2}(y)}, \frac{1}{m_{3}(z)}\right) - w_{0}(\mathbf{x}, t_{0}),$$

$$\tau_{2}(\mathbf{x}; t_{0}; \boldsymbol{\xi}) = \frac{\boldsymbol{\xi}}{2} \cdot \left(\frac{(w_{0})_{x}}{m_{1}(x)}, \frac{(w_{0})_{y}}{m_{2}(y)}, \frac{(w_{0})_{z}}{m_{3}(z)}\right) - \frac{\boldsymbol{\xi}^{3}}{4} \cdot \left(\frac{m'_{1}(x)}{m_{1}^{3}(x)}, \frac{m'_{2}(y)}{m_{3}^{3}(y)}, \frac{m'_{3}(z)}{m_{3}^{3}(z)}\right) - \frac{w_{1}(\mathbf{x}, t_{0})}{2},$$

and similarly for $\tau_l(\mathbf{x}; t_0; \boldsymbol{\xi})$ with $l \geq 3$ as

(2.13) $\tau_l(\mathbf{x}; t_0; \boldsymbol{\xi})$

$$= \frac{1}{l} \left\{ -w_l(\mathbf{x}, t_0) - \sum_{s=0}^{l-1} \left(\frac{(\tau_s)_x (\tau_{l-1-s})_x}{2m_1(x)} + \frac{(\tau_s)_y (\tau_{l-1-s})_y}{2m_2(y)} + \frac{(\tau_s)_z (\tau_{l-1-s})_z}{2m_3(z)} \right) \right\}.$$

By substituting the Taylor series for A_0 into the transport equation (2.9) and collecting the terms of the same order in Δt , we have

(2.14)

 $A_{00}(\mathbf{x}; t_0; \boldsymbol{\xi}) = 1,$

 $A_{01}(\mathbf{x}; t_0; \boldsymbol{\xi}) = 0,$

$$\begin{split} A_{02}(\mathbf{x};t_0;\pmb{\xi}) = & -\frac{1}{8} \left(\frac{m_1(x)''}{m_1^3(x)} + \frac{m_2''(y)}{m_2^3(y)} + \frac{m_3''(z)}{m_3^3(z)} - \frac{2(m_1'(x))^2}{m_1^4(x)} - \frac{2(m_2'(y))^2}{m_2^4(y)} - \frac{2(m_3'(z))^2}{m_3^4(z)} \right) \\ & + \frac{1}{4} \left(\frac{(w_0)_{xx}}{m_1(x)} + \frac{(w_0)_{yy}}{m_2(y)} + \frac{(w_0)_{zz}}{m_3(z)} \right), \end{split}$$

and similarly for $A_{0l}(\mathbf{x}; t_0; \boldsymbol{\xi})$ with $l \geq 3$ as

(2.15)

$$A_{0l}(\mathbf{x}; t_0; \boldsymbol{\xi}) = \frac{1}{l} \left\{ -\sum_{s=0}^{l-1} \left(\frac{(A_{0s})_x (\tau_{l-1-s})_x}{m_1(x)} + \frac{(A_{0s})_y (\tau_{l-1-s})_y}{m_2(y)} + \frac{(A_{0s})_z (\tau_{l-1-s})_z}{m_3(z)} \right) - \sum_{s=0}^{l-1} \left(\frac{A_{0s} (\tau_{l-1-s})_{xx}}{2m_1(x)} + \frac{A_{0s} (\tau_{l-1-s})_{yy}}{2m_2(y)} + \frac{A_{0s} (\tau_{l-1-s})_{zz}}{2m_3(z)} \right) \right\}.$$

By substituting the Taylor series for A_k with $k \geq 1$ into the transport equation (2.10) and collecting the terms of the same order in Δt , we have

(2.16)
$$A_{k0}(\mathbf{x}; t_0; \boldsymbol{\xi}) = 0,$$

$$A_{k1}(\mathbf{x}; t_0; \boldsymbol{\xi}) = 0,$$

$$A_{k2}(\mathbf{x}; t_0; \boldsymbol{\xi}) = 0,$$

and similarly for $A_{kl}(\mathbf{x}; t_0; \boldsymbol{\xi})$ with $l \geq 3$ as

(2.17)

$$A_{kl}(\mathbf{x}; t_0; \boldsymbol{\xi}) = \frac{1}{l} \left\{ -\sum_{s=0}^{l-1} \left(\frac{(A_{ks})_x (\tau_{l-1-s})_x}{m_1(x)} + \frac{(A_{ks})_y (\tau_{l-1-s})_y}{m_2(y)} + \frac{(A_{ks})_z (\tau_{l-1-s})_z}{m_3(z)} \right) - \sum_{s=0}^{l-1} \left(\frac{A_{ks} (\tau_{l-1-s})_{xx}}{2m_1(x)} + \frac{A_{ks} (\tau_{l-1-s})_{yy}}{2m_2(y)} + \frac{A_{ks} (\tau_{l-1-s})_{zz}}{2m_3(z)} \right) - \sum_{s=0}^{l-1} \left(\frac{1}{2m_1(x)} (A_{k-1,s})_{xx} + \frac{1}{2m_2(y)} (A_{k-1,s})_{yy} + \frac{1}{2m_3(z)} (A_{k-1,s})_{zz} \right) \right\}.$$

Therefore, analytic approximations of τ and $\{A_k\}_{k=0}^{\infty}$ for a short period of time can be obtained with the Taylor series (2.11).

2.4. Algorithms. With the short-time analytic approximations of τ and $\{A_k\}_{k=0}^{\infty}$, we demonstrate how to implement the asymptotic short-time propagator with the following approximation:

(2.18)
$$\tau = \tau_0 + \tau_1 \Delta t + O(\Delta t^2), A = A_{00} + A_{01} \Delta t + O(\Delta t^2) + O(\hbar).$$

In particular, we will approximate the wavefunction $\psi(\mathbf{x},t)$ as

(2.19)
$$\psi(\mathbf{x},t) \approx \int_{\mathbf{R}^3} \exp(\iota \tau(\mathbf{x},t;t_0;\boldsymbol{\xi})/\hbar) A_0(\mathbf{x},t;t_0;\boldsymbol{\xi}) \hat{\psi}(\boldsymbol{\xi},t_0) d\boldsymbol{\xi},$$

with the phase τ and the amplitude A_0 approximated as

(2.20)

$$\tau(\mathbf{x}, t; t_0; \boldsymbol{\xi}) = \boldsymbol{\xi} \cdot \mathbf{x} - \left\{ \frac{\boldsymbol{\xi}^2}{2} \cdot \left(\frac{1}{m_1(x)}, \frac{1}{m_2(y)}, \frac{1}{m_3(z)} \right) + w_0 \right\} \Delta t + O(\Delta t^2),$$

$$A_0(\mathbf{x}, t; t_0; \boldsymbol{\xi}) = 1 + O(\Delta t^2).$$

Formulas (2.19) and (2.20) yield a first-order approximation for $\psi(\mathbf{x},t) = \psi(\mathbf{x},t_0+\Delta t)$:

(2.21)
$$\psi(\mathbf{x},t) = \exp\left(\frac{-\iota w_0(\mathbf{x},t_0)\Delta t}{\hbar}\right) \int_{\mathbf{R}^3} \exp\left(\frac{\iota \mathbf{x} \cdot \boldsymbol{\xi}}{\hbar}\right) \times \exp\left(\frac{-\iota \Delta t}{2\hbar} \left(\frac{\xi_1^2}{m_1(x)} + \frac{\xi_2^2}{m_2(y)} + \frac{\xi_3^2}{m_3(z)}\right)\right) \hat{\psi}(\boldsymbol{\xi},t_0) d\boldsymbol{\xi} + O(\Delta t^2 (1+\hbar)),$$

which provides the short-time propagator for the wavefunction ψ in the semiclassical regime.

If \mathbf{x} is not in the PMLs, (2.21) reads

(2.22)
$$\psi(\mathbf{x},t) = \exp\left(\frac{-\iota w_0(\mathbf{x},t_0)\Delta t}{\hbar}\right) \int_{\mathbf{R}^3} \exp\left(\frac{\iota \mathbf{x} \cdot \boldsymbol{\xi}}{\hbar}\right) \exp\left(\frac{-\iota \Delta t}{2m\hbar} \boldsymbol{\xi}^2\right) \hat{\psi}(\boldsymbol{\xi},t_0) d\boldsymbol{\xi} + O(\Delta t^2 (1+\hbar))$$

$$= \exp\left(\frac{-\iota w_0(\mathbf{x},t_0)\Delta t}{\hbar}\right) \mathcal{F}^{-1} \left[\exp\left(\frac{-\iota \boldsymbol{\xi}^2 \Delta t}{2m\hbar}\right) \mathcal{F}[\psi(\mathbf{x},t_0)]\right] + O(\Delta t^2 (1+\hbar)),$$

with \mathcal{F}^{-1} the inverse Fourier transform defined as

$$\mathcal{F}^{-1}[\hat{\psi}(\boldsymbol{\xi}, t_0)] = \int_{\mathbf{R}^3} \exp\left(\frac{\iota \mathbf{x} \cdot \boldsymbol{\xi}}{\hbar}\right) \hat{\psi}(\boldsymbol{\xi}, t_0) d\boldsymbol{\xi}.$$

We can discretize the Fourier transform (2.7) as

(2.23)
$$\hat{\psi}_{ijk}(t_0) = \frac{\Delta xyz}{(2\pi\hbar)^3} \sum_{ii,ji,kk} \exp\left(\frac{-\iota \mathbf{x}_{iijjkk} \cdot \boldsymbol{\xi}_{ijk}}{\hbar}\right) \psi_{iijjkk}(t_0),$$

the integral (2.21) as

(2.24)
$$\psi_{iijjkk}(t) = \exp\left(\frac{-\iota w_{0,iijjkk}(t_0)\Delta t}{\hbar}\right) \Delta \xi_1 \xi_2 \xi_3 \sum_{i,j,k} \exp\left(\frac{\iota \mathbf{x}_{iijjkk} \cdot \boldsymbol{\xi}_{ijk}}{\hbar}\right) \times \exp\left(\frac{-\iota \Delta t}{2\hbar} \left(\frac{\xi_{1i}^2}{m_{1,ii}} + \frac{\xi_{2j}^2}{m_{2,jj}} + \frac{\xi_{3k}^2}{m_{3,kk}}\right)\right) \hat{\psi}_{ijk}(t_0),$$

and the integral (2.22) as

(2.25)
$$\psi_{iijjkk}(t) = \exp\left(\frac{-\iota w_{0,iijjkk}(t_0)\Delta t}{\hbar}\right) \Delta \xi_1 \xi_2 \xi_3 \sum_{i,j,k} \exp\left(\frac{\iota \mathbf{x}_{iijjkk} \cdot \boldsymbol{\xi}_{ijk}}{\hbar}\right) \times \exp\left(\frac{-\iota \Delta t}{2\hbar} \left(\frac{\boldsymbol{\xi}_{ijk}^2}{m}\right)\right) \hat{\psi}_{ijk}(t_0),$$

with $\hat{\psi}_{ijk}(t_0) = \hat{\psi}(\boldsymbol{\xi}_{ijk}, t_0), \psi_{iijjkk}(t_0) = \psi(\mathbf{x}_{iijjkk}, t_0), \boldsymbol{\xi}_{ijk} = (\xi_{1i}, \xi_{2j}, \xi_{3k}), \mathbf{x}_{iijjkk} = (x_{ii}, y_{jj}, z_{kk}), \ \Delta xyz = \Delta x \Delta y \Delta z, \ w_{0,iijjkk}(t_0) = w_0(\mathbf{x}_{iijjkk}, t_0), m_{1,ii} = m_1(x_{ii}), m_{2,jj} = m_2(y_{jj}), m_{3,kk} = m_3(z_{kk}), \text{ and } \Delta \xi_1 \xi_2 \xi_3 = \Delta \xi_1 \Delta \xi_2 \Delta \xi_3.$

The formula (2.23) for approximating the Fourier transform and the formula (2.25) for computing ψ with \mathbf{x} not in the PMLs can be implemented efficiently by the FFT [14]. And the formula (2.21) and/or (2.24) for computing ψ with \mathbf{x} in the PMLs can be implemented by direct summation. Therefore, we have first algorithm for computing the wavefunction ψ .

Algorithm 1 (Direct sum for \mathbf{x} in PMLs).

For k = 0, 1, 2, ...:

- 1. At $t_0 = k\Delta t$, apply FFT and (2.23) to compute $\hat{\psi}(\boldsymbol{\xi}, t_0) = \mathcal{F}[\psi(\boldsymbol{x}, t_0)]$;
- 2. At $t = t_0 + \Delta t$:
 - (a) for \mathbf{x} not in the PMLs, apply FFT and (2.25) to compute $\psi(\mathbf{x},t)$:
 - apply FFT to compute

$$W_{iijjkk} \equiv \Delta \xi_1 \xi_2 \xi_3 \sum_{i,j,k} \exp\left(\frac{\iota \mathbf{x}_{iijjkk} \cdot \mathbf{\xi}_{ijk}}{\hbar}\right) \hat{W}_{ijk}$$

with
$$\hat{W}_{ijk} = \exp\left(\frac{-\iota \Delta t}{2\hbar} \left(\frac{\boldsymbol{\xi}_{ijk}^2}{m}\right)\right) \hat{\psi}_{ijk}(t_0);$$

• compute

$$\psi_{iijjkk}(t) = \exp\left(\frac{-\iota w_{0,iijjkk}(t_0)\Delta t}{\hbar}\right) W_{iijjkk}.$$

(b) for \mathbf{x} in the PMLs, apply (2.24) to compute $\psi(\mathbf{x},t)$ with direct summation.

For Algorithm 1, the complexity of step 1 and part (a) of step 2 is $O(N \log N)$ with $N = N_x N_y N_z$ since FFT is applied. The complexity of part (b) of step 2 is $O(\frac{\eta_x}{\hbar}, \frac{\eta_y}{\hbar}, \frac{\eta_z}{\hbar}, M_x M_y M_z N)$, provided that $\Delta x = O(\frac{\hbar}{M_x})$, $\Delta y = O(\frac{\hbar}{M_y})$, and $\Delta z = O(\frac{\hbar}{M_z})$ for certain constants M_x, M_y , and M_z . Therefore, the total complexity is $O(N \log N + \frac{\eta_x}{\hbar}, \frac{\eta_y}{\hbar}, \frac{\eta_z}{\hbar}, MN)$ with $M = M_x M_y M_z$, which depends on the width of the PMLs.

The complexity for computing $\psi(\mathbf{x},t)$ with \mathbf{x} in the PMLs can become too high with small parameter \hbar if the width of the PMLs is independent of \hbar . Fortunately, we find that the following term,

(2.26)

$$\begin{split} E(\mathbf{x}, \boldsymbol{\xi}) &\equiv \exp\left(\frac{-\iota \Delta t}{2\hbar} \left(\frac{\xi_1^2}{m_1(x)} + \frac{\xi_2^2}{m_2(y)} + \frac{\xi_3^2}{m_3(z)}\right)\right) \\ &= \exp\left(\frac{-\iota \Delta t}{2\hbar} \left(\frac{\xi_1^2}{m_1(x)}\right)\right) \exp\left(\frac{-\iota \Delta t}{2\hbar} \left(\frac{\xi_2^2}{m_2(y)}\right)\right) \exp\left(\frac{-\iota \Delta t}{2\hbar} \left(\frac{\xi_3^2}{m_3(z)}\right)\right), \end{split}$$

is not oscillatory with respect to \mathbf{x} when $\boldsymbol{\xi}$ is in a bounded domain and Δt is small enough. Consequently we can apply a low-rank approximation of this term, e.g., with piecewise Chebyshev polynomial interpolation [11, 15, 23, 27, 28], given as

(2.27)
$$E(\mathbf{x}, \boldsymbol{\xi}) \approx \sum_{p=1}^{C_p} \sum_{q=1}^{C_q} \sum_{r=1}^{C_r} L(x, x_p) L(y, y_q) L(z, z_r) E(\mathbf{x}_{pqr}, \boldsymbol{\xi}),$$

where $\{\mathbf{x}_{pqr} \equiv (x_p, y_q, z_r)\} \equiv \{x_p\}_{p=1}^{C_p} \times \{y_q\}_{q=1}^{C_q} \times \{z_r\}_{r=1}^{C_r}$ are Chebyshev nodes in Ω , and $L(\cdot, \cdot)$ is the Lagrange basis function. C_p, C_q , and C_r are expected to be much smaller than N_x, N_y , and N_z .

With the piecewise Chebyshev polynomial interpolation, we can approximate (2.21) as

(2.28)

$$\psi(\mathbf{x},t) \approx \exp\left(\frac{-\iota w_0(\mathbf{x},t_0)\Delta t}{\hbar}\right) \int_{\mathbf{R}^3} \exp\left(\frac{\iota \mathbf{x} \cdot \boldsymbol{\xi}}{\hbar}\right) \left\{ \sum_{p=1}^{C_p} L(x,x_p) \exp\left(\frac{-\iota \Delta t \boldsymbol{\xi}_1^2}{2m_1(x_p)\hbar}\right) \right\}$$

$$\times \left\{ \sum_{q=1}^{C_q} L(y,y_q) \exp\left(\frac{-\iota \Delta t \boldsymbol{\xi}_1^2}{2m_2(y_q)\hbar}\right) \right\} \left\{ \sum_{r=1}^{C_r} L(z,z_r) \exp\left(\frac{-\iota \Delta t \boldsymbol{\xi}_1^2}{2m_3(z_r)\hbar}\right) \right\} \hat{\psi}(\boldsymbol{\xi},t_0) d\boldsymbol{\xi}$$

$$= \exp\left(\frac{-\iota w_0(\mathbf{x},t_0)\Delta t}{\hbar}\right) \sum_{p=1}^{C_p} \sum_{q=1}^{C_q} \sum_{r=1}^{C_r} L(x,x_p)L(y,y_q)L(z,z_r)$$

$$\times \int_{\mathbf{R}^3} \exp\left(\frac{\iota \mathbf{x} \cdot \boldsymbol{\xi}}{\hbar}\right) E(\mathbf{x}_{pqr},\boldsymbol{\xi}) \hat{\psi}(\boldsymbol{\xi},t_0) d\boldsymbol{\xi}$$

$$= \exp\left(\frac{-\iota w_0(\mathbf{x},t_0)\Delta t}{\hbar}\right) \sum_{p=1}^{C_p} \sum_{q=1}^{C_q} \sum_{r=1}^{C_r} L(x,x_p)L(y,y_q)L(z,z_r)$$

$$\times \mathcal{F}^{-1} \left[E(\mathbf{x}_{pqr},\boldsymbol{\xi})\mathcal{F}[\psi(\mathbf{x},t_0)]\right]$$

and (2.25) as

$$\psi_{iijjkk}(t) \approx \exp\left(\frac{-\iota w_{0,iijjkk}(t_0)\Delta t}{\hbar}\right) \sum_{p=1}^{C_p} \sum_{q=1}^{C_q} \sum_{r=1}^{C_r} L(x_{ii}, x_p) L(y_{jj}, y_q) L(z_{kk}, z_r)$$
$$\times \Delta \xi_1 \xi_2 \xi_3 \sum_{i,j,k} \exp\left(\frac{\iota \mathbf{x}_{iijjkk} \cdot \boldsymbol{\xi}_{ijk}}{\hbar}\right) E(\mathbf{x}_{pqr}, \boldsymbol{\xi}_{ijk}) \hat{\psi}_{ijk}(t_0).$$

With the low-rank approximation by piecewise Chebyshev polynomial interpolation, formulas (2.28) and/or (2.29) can be evaluated efficiently because the FFT can be utilized. Therefore, we have second algorithm for computing the wavefunction ψ :

Algorithm 2 (low-rank approximation via Chebyshev polynomial interpolation).

For k = 0, 1, 2, ...:

- 1. At $t_0 = k\Delta t$, apply FFT and (2.23) to compute $\hat{\psi}(\boldsymbol{\xi}, t_0) = \mathcal{F}[\psi(\boldsymbol{x}, t_0)]$;
- 2. At $t = t_0 + \Delta t$, apply FFT and (2.29) to compute $\psi(\mathbf{x}, t)$:
 - (a) for each Chebyshev node $\mathbf{x}_{pqr} = (x_p, y_q, z_r)$, apply FFT to compute

$$W_{pqr}^{iijjkk} \equiv \Delta \xi_1 \xi_2 \xi_3 \sum_{i,j,k} \exp\left(\frac{\iota \mathbf{\textit{x}}_{iijjkk} \cdot \mathbf{\textit{\xi}}_{ijk}}{\hbar}\right) \hat{W}_{ijk}$$

with $\hat{W}_{ijk} = E(\mathbf{x}_{pqr}, \boldsymbol{\xi}_{ijk}) \hat{\psi}_{ijk}(t_0);$ (b) compute $\psi(\mathbf{x}, t)$ as

$$\psi_{iijjkk}(t) \approx \exp\left(\frac{-\iota w_{0,iijjkk}(t_0)\Delta t}{\hbar}\right)$$
$$\sum_{p=1}^{C_p} \sum_{q=1}^{C_q} \sum_{r=1}^{C_r} L(x_{ii}, x_p) L(y_{jj}, y_q) L(z_{kk}, z_r) W_{pqr}^{iijjkk}.$$

For Algorithm 2, the complexity of step 1 is $O(N \log N)$, the complexity of part (a) of step 2 is $O(C_{pqr}N \log N)$ with $C_{pqr} = C_pC_qC_r$, and the complexity of part (b) of step 2 is $O(C_{pqr}N)$. Therefore the total complexity is $O(N \log N + C_{pqr}N \log N + C_{pqr}N)$, which is independent of the width of the PMLs.

The efficiency of Algorithm 2 also depends on the piecewise Chebyshev polynomial interpolation of the term $E(\mathbf{x}, \boldsymbol{\xi})$ defined in (2.26). For notational simplicity, we focus on the first factor $E_1(x, \xi_1) \equiv \exp(\frac{-\iota \Delta t}{2\hbar} (\frac{\xi_1^2}{m_1(x)}))$, and explain how to perform the piecewise Chebyshev polynomial interpolation.

The Chebyshev nodes on [-1, 1] are given as

$$\tilde{t}_{n,k} = \cos\left(\frac{2k-1}{2n}\pi\right), \ k = 1, 2, \dots, n,$$

and they can be mapped to any interval [a, b] as

$$t_{n,k}^{(a,b)} = \frac{a+b}{2} + \frac{b-a}{2}\tilde{t}_{n,k}, \ k = 1, 2, \dots, n.$$

By examining the function $E_1(x, \xi_1)$, we note that it is constant for x not in the PMLs, i.e.,

$$E_1(x,\xi_1) = \exp\left(\frac{-\iota \Delta t}{2\hbar} \left(\frac{\xi_1^2}{m}\right)\right) \forall x \in [x_{\min} + \eta_x, \ x_{\max} - \eta_x].$$

Therefore, we can apply piecewise polynomial interpolation on $[x_{\min}, x_{\max}]$ with three subintervals $\{[x_{\min}, x_{\min} + \eta_x], [x_{\min} + \eta_x, x_{\max} - \eta_x], [x_{\max} - \eta_x, x_{\max}]\}$ (Figure 2a), and choose the interpolation nodes as

$$\left\{x_{p}\right\}_{p=1}^{C_{p}} \equiv \left\{t_{C_{p}',k}^{(x_{\min}, x_{\min} + \eta_{x})}\right\}_{k=1}^{C_{p}'} \bigcup \left\{\frac{x_{\min} + x_{\max}}{2}\right\} \bigcup \left\{t_{C_{p}',k}^{(x_{\max} - \eta_{x}, x_{\max})}\right\}_{k=1}^{C_{p}'},$$

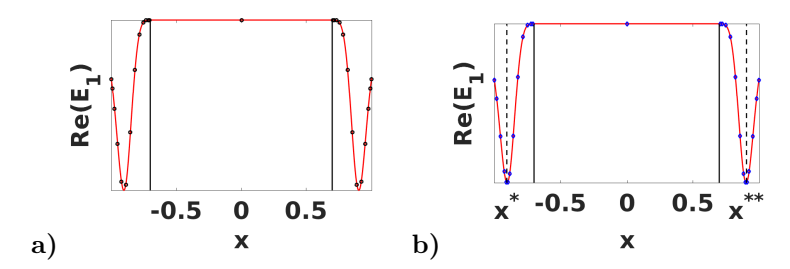


FIG. 2. Demonstration of Chebyshev nodes for piecewise polynomial interpolation. Solid red curve indicates the function. Vertical solid lines indicate boundaries of PMLs. (a) three subintervals $[x_{\min}, x_{\min} + \eta_x]$, $[x_{\min} + \eta_x, x_{\max} - \eta_x]$, and $[x_{\max} - \eta_x, x_{\max}]$, black circles indicate Chebyshev nodes in the corresponding subintervals; (b) five subintervals $[x_{\min}, x^*]$, $[x^*, x_{\min} + \eta_x]$, $[x_{\max} - \eta_x, x^{**}]$, and $[x^{**}, x_{\max}]$, blue circles indicate Chebyshev nodes in the corresponding subintervals.

with $C_p' = (C_p - 1)/2$. That is, we can use Chebyshev polynomial interpolation on $[x_{\min}, x_{\min} + \eta_x]$ and $[x_{\max} - \eta_x, x_{\max}]$, respectively, and use constant polynomial approximation on $[x_{\min} + \eta_x, x_{\max} - \eta_x]$. Similarly, we can choose

$$\{y_q\}_{q=1}^{C_q} \equiv \left\{t_{C_q',k}^{(y_{\min},\ y_{\min}+\eta_y)}\right\}_{k=1}^{C_q'} \bigcup \left\{\frac{y_{\min}+y_{\max}}{2}\right\} \bigcup \left\{t_{C_q',k}^{(y_{\max}-\eta_y,\ y_{\max})}\right\}_{k=1}^{C_q'},$$

$$\{z_r\}_{r=1}^{C_r} \equiv \left\{t_{C_r',k}^{(z_{\min},\ z_{\min}+\eta_z)}\right\}_{k=1}^{C_r'} \bigcup \left\{\frac{z_{\min}+z_{\max}}{2}\right\} \bigcup \left\{t_{C_r',k}^{(z_{\max}-\eta_z,\ z_{\max})}\right\}_{k=1}^{C_r'},$$
 with $C_q' = (C_q-1)/2, C_r' = (C_r-1)/2.$

Remark 2.1. By further examining the function $E_1(x, \xi_1)$, we note that it is possible to perform piecewise polynomial interpolation with more subintervals to capture more detailed features of the function, which requires more rigorous analysis and will not be discussed in this work. However, we will also perform numerical experiments with the following choice of Chebyshev nodes (Figure 2b),

$$\begin{aligned}
\{x_p\}_{p=1}^{C_p} &\equiv \left\{t_{C_p,k}^{(x_{\min}, x^{\star})}\right\}_{k=1}^{C_p^1} \bigcup \left\{t_{C_p,k}^{(x^{\star}, x_{\min} + \eta_x)}\right\}_{k=1}^{C_p^2} \\
&\qquad \qquad \bigcup \left\{\frac{x_{\min} + x_{\max}}{2}\right\} \\
&\qquad \qquad \bigcup \left\{t_{C_p,k}^{(x_{\max} - \eta_x, x^{\star^{\star}})}\right\}_{k=1}^{C_p^2} \bigcup \left\{t_{C_p,k}^{(x^{\star^{\star}}, x_{\max})}\right\}_{k=1}^{C_p^1},
\end{aligned}$$

with $C_p = 2(C_p^1 + C_p^2) + 1$. $\{y_q\}_{q=1}^{C_q}$ and $\{z_r\}_{r=1}^{C_r}$ can be chosen similarly.

2.5. Applications to Gross-Pitaevskii equations. We can apply Algorithms 1 and 2 to compute the wavefunction for the time-dependent Gross-Pitaevskii equation that describes the dynamics of a trapped Bose-Einstein condensates (BEC) at zero temperature [6, 12]:

(2.32)
$$\iota\hbar\frac{\partial\phi(\mathbf{x},t)}{\partial t} = -\frac{\hbar^2}{2m}\nabla^2\phi(\mathbf{x},t) + v(\mathbf{x},t)\phi(\mathbf{x},t) + MU_0|\phi(\mathbf{x},t)|^2\phi(\mathbf{x},t), \ t > 0,$$
$$\phi(\mathbf{x},0) = \phi_0(\mathbf{x}),$$

where $U_0 = 4\pi\hbar^2 a/m$ is the coupling strength, a is the scattering length, and M is the number of particles in the condensate. With the PMLs, the modified Gross-Pitaevskii equation has the form (2.2), with

$$w(\mathbf{x},t) = -\frac{\hbar^2}{2m} \left(\frac{(s_1'(x))^2 + (s_2'(y))^2 + (s_3'(z))^2}{4} - \frac{s_1(x)s_1''(x) + s_2(y)s_2''(y) + s_3(z)s_3''(z)}{2} \right) + v(\mathbf{x},t) + MU_0 \left| \frac{\psi^2(\mathbf{x},t)}{s_1(x)s_2(y)s_3(z)} \right|.$$

2.6. Discussion of Algorithms 1 and 2. The complexity of Algorithm 1 is $O(N \log N + \frac{\eta_x \eta_y \eta_z}{\hbar^3} MN)$ with $N = N_x N_y N_z$ and $M = M_x M_y M_z$, provided that $\Delta x = O(\frac{\hbar}{M_x}), \Delta y = O(\frac{\hbar}{M_y}), \Delta z = O(\frac{\hbar}{M_z})$. The complexity depends on the width of the PMLs. If the width of the PMLs is independent of \hbar , then the second term is dominant as $\hbar \to 0$, and the complexity becomes too high. If the width of the PMLs is $O(\hbar)$, i.e., $\eta_x = O(\hbar), \eta_y = O(\hbar), \eta_z = O(\hbar)$, then the complexity is as low as $O(N \log N + MN)$.

The complexity of Algorithm 2 is as low as $O(N \log N + C_{pqr} N \log N + C_{pqr} N)$ with $C_{pqr} = C_p C_q C_r$. The complexity depends on the numbers of the Chebyshev nodes. For certain accuracy requirement, the numbers of the Chebyshev nodes are independent of \hbar as $\hbar \to 0$.

We demonstrate the algorithms with numerical experiments.

3. Numerical examples. We present one-dimensional (1-D) and two-dimensional (2-D) examples to demonstrate the proposed methods. The reference solutions are computed with the spectral Strang operator splitting method [6, 30], where the solutions are assumed to be compactly supported in the computational domain. For simplicity, we consider the following dimensionless equations after appropriate change of variables:

(3.1)
$$\iota \epsilon \frac{\partial \phi(\mathbf{x}, t)}{\partial t} = -\frac{\epsilon^2}{2} \nabla^2 \phi(\mathbf{x}, t) + v(\mathbf{x}, t) \phi(\mathbf{x}, t) + \kappa |\phi(\mathbf{x}, t)|^2 \phi(\mathbf{x}, t),$$

where ϵ is the small parameter and κ is constant. The proposed methods and the spectral Strang operator splitting method are implemented with Matlab on a Linux desktop. We will denote Algorithm 2 with Chebyshev nodes chosen in (2.31) as Algorithm 2(a), and denote Algorithm 2 with Chebyshev nodes chosen in (2.30) as Algorithm 2(b).

Example 1 (1-D examples). We present 1-D examples to check efficiency and accuracy of the proposed methods:

• The potential is

$$v(x,t) = \frac{x^2}{2} + 20\cos(20\pi t)\exp(-x^2/2).$$

• The initial condition is

$$\phi(x,0) = \exp(-x^2/0.02).$$

- The computational domain for the proposed method is $[-1 \ 1]$, and the computational domain for the reference solution is $[-4 \ 4]$.
- Both the errors and CPU time for computing the solutions up to time t=0.5 are recorded.

Tables 1 and 2 show the l_{∞} and l_2 errors between the solutions computed by the proposed methods and the reference solutions. First-order accuracy, i.e., $O(\Delta x +$

 Δt), of the proposed methods is observed. Tables 3 and 4 show the l_{∞} and l_2 errors between the solutions computed by Algorithm 1 and Algorithm 2(a), and between the solutions computed by Algorithm 1 and Algorithm 2(b). Stability of the low-rank approximation with piecewise Chebyshev polynomial interpolation is observed, since the errors between Algorithm 1 and Algorithm 2 do not increase as ϵ decreases, and the number of Chebyshev nodes is fixed. Furthermore, from the CPU time recorded in these tables, $O(N \log N)$ complexity of Algorithm 2 is observed. For Algorithm 1, if the width of the PMLs depends on \hbar , $O(N \log N)$ complexity is observed; if the width of the PMLs is independent of \hbar , $O(N^2)$ complexity is observed.

Figures 3 and 4 show the plots of the numerical solutions ϕ , Figure 5 shows the plots of $|\phi|^2$, and Figure 6 shows the plots of $\int |\phi|^2 dx$.

Table 1 1-D example, order of accuracy, and CPU time. l_{∞} error, l_{2} error, and CPU time are recorded. For the reference solution, $\Delta x = \epsilon/64$, $\Delta t = \Delta x/16$; and for the proposed methods, $\Delta t = \Delta x/16$.

$\epsilon = 0.025, \kappa = -1, C_p = 13; C_x = 2.5; \eta_x = 0.3$					
Δx	$\epsilon/4$	$\epsilon/8$	$\epsilon/16$	$\epsilon/32$	
Alg. 1: l_{∞} Err.	9.551E-2	2.079E-2	6.516E-3	2.261E-3	
Conv. Order	-	2.200	1.674	1.527	
Alg. 1: l_2 Err.	1.637E-2	3.727E-3	1.221E-3	4.401E-4	
Conv. Order	-	2.135	1.610	1.472	
CPU time	1.696E1	3.511E1	9.202E1	2.686E2	
Alg. $2(a)$: l_{∞} Err.	9.551E-2	2.079E-2	6.516E-3	2.261E-3	
Conv. Order	-	2.200	1.674	1.527	
Alg. $2(a)$: l_2 Err.	1.637E-2	3.727E-3	1.221E-3	4.401E-4	
Conv. Order	-	2.135	1.610	1.472	
CPU time	1.709E1	3.467E1	9.281E1	1.714E2	
Alg. 2(b): l_{∞} Err.	9.551E-2	2.079E-2	6.516E-3	2.261E-3	
Conv. Order	_	2.200	1.674	1.527	
Alg. 2(b): l_2 Err.	1.637E-2	3.727E-3	1.221E-3	4.401E-4	
Conv. Order	_	2.135	1.610	1.472	
CPU time	1.708E1	3.459E1	9.287E1	2.035E2	
$\epsilon = 0.01,$	$\kappa = 2, C_p =$	$= 13; C_x = 2.$	$.5; \eta_x = 0.3$		
Δx	$\epsilon/4$	$\epsilon/8$	$\epsilon/16$	$\epsilon/32$	
Alg. 1: l_{∞} Err.	6.559E-3	3.279E-3	1.639E-3	8.195E-4	
Conv. Order	_	1.000	1.000	1.000	
Alg. 1: l_2 Err.	3.972E-3	1.982E-3	9.900E-4	4.948E-4	
Conv. Order	_	1.003	1.001	1.001	
CPU time	6.057E1	1.368E2	3.853E2	1.308E3	
Alg. $2(a)$: l_{∞} Err.	6.566E-3	3.295E-3	1.660E-3	8.423E-4	
Conv. Order	_	0.995	0.989	0.979	
Alg. $2(a)$: l_2 Err.	3.972E-3	1.982E-3	9.904E-4	4.952E-4	
0 0 1		1.003	1.001	1.000	
Conv. Order	_	1.005	1.001	1.000	
Conv. Order CPU time	5.780E1	1.005 1.196E2	2.483E2	5.552E2	
	5.780E1 6.569E-3				
CPU time		1.196E2	2.483E2	5.552E2	
CPU time Alg. 2(b): l_{∞} Err. Conv. Order Alg. 2(b): l_2 Err.		1.196E2 3.289E-3	2.483E2 1.650E-3	5.552E2 8.297E-4	
CPU time Alg. $2(b)$: l_{∞} Err. Conv. Order	6.569E-3 -	1.196E2 3.289E-3 0.998	2.483E2 1.650E-3 0.995	5.552E2 8.297E-4 0.992	

Example 2 (2-D examples). We demonstrate the performance of the proposed methods with the following 2-D examples.

• Case 1: the potential is

$$v(x, y, t) = \frac{x^2 + y^2}{2} + 2\cos(2\pi t)\exp(-(x^2 + y^2)/2),$$

Table 2

1-D example, order of accuracy, and CPU time. l_{∞} error, l_2 error, and CPU time are recorded. For the reference solution, $\Delta x = \epsilon/64$, $\Delta t = \Delta x/16$; and for the proposed methods, $\Delta t = \Delta x/16$.

$\kappa = 2, C_p = 13; C_x = 5; \eta_x = \min(30\epsilon, 0.3)$					
$\epsilon (\Delta x)$	$0.04 \ (\epsilon/2)$	$0.02 \ (\epsilon/4)$	$0.01 \ (\epsilon/8)$	$0.005 \ (\epsilon/16)$	
Alg. 1: l_{∞} Err.	1.380E-2	6.614E-3	3.279E-3	1.636E-3	
Conv. Order	_	1.061	1.012	1.003	
Alg. 1: l_2 Err.	8.300E-3	4.008E-3	1.982E-3	9.883E-4	
Conv. Order	_	1.050	1.016	1.004	
CPU time	7.660	2.585E1	9.589E1	7.802E2	
Alg. $2(a)$: l_{∞} Err.	1.399E-2	6.572E-3	3.287E-3	1.644E-3	
Conv. Order	_	1.090	1.000	1.000	
Alg. $2(a)$: l_2 Err.	8.306E-3	4.007E-3	1.982E-3	9.883E-4	
Conv. Order	_	1.052	1.016	1.004	
CPU time	7.545	2.515E1	9.290E1	4.338E2	
Alg. 2(b): l_{∞} Err.	1.379E-2	6.605E-3	3.292E-3	1.650E-3	
Conv. Order	_	1.062	1.005	0.996	
Alg. 2(b): l_2 Err.	8.301E-3	4.006E-3	1.983E-3	9.884E-4	
Conv. Order	_	1.051	1.014	1.005	
CPU time	7.308	2.694E1	9.372E1	4.324E2	

Table 3

1-D example, stability, and CPU time. l_{∞} error, l_2 error, and CPU time are recorded. For the proposed methods, $\Delta t = \Delta x/16$.

$\Delta x = \epsilon/8, \kappa = 2, C_p = 13; C_x = 0.5; \eta_x = \min(30\epsilon, 0.3)$					
ϵ	0.04	0.02	0.01	0.005	0.0025
CPU time for Alg. 1	2.691E1	5.500E1	1.274E2	2.193E2	4.926E2
CPU time for Alg. 2(a)	2.867E1	4.842E1	9.084E1	1.476E2	4.371E2
CPU time for Alg. 2(b)	3.094E1	5.486E1	1.193E2	1.568E2	4.351E2
Alg. $2(a)$: l_{∞} Err.	4.680E-4	4.088E-4	2.395E-4	2.025E-4	1.739E-4
Alg. $2(a)$: l_2 Err.	2.238E-4	1.209E-4	5.264E-5	3.217E-5	2.073E-5
Alg. 2(b): l_{∞} Err.	9.054E-5	7.059E-5	8.877E-5	8.175E-5	7.614E-5
Alg. $2(b)$: l_2 Err.	6.978E-5	4.820E-5	4.074E-5	2.587E-5	1.820E-5
$\Delta x = \epsilon/8, \kappa = 2, C_p = 13; C_x = 2.5; \eta_x = 0.3$					
ϵ	0.04	0.02	0.01	0.005	0.0025
CPU time for Alg. 1	2.472E1	5.057E1	1.161E2	3.237E2	1.021E3
CPU time for Alg. 2(a)	2.388E1	4.943E1	1.018E2	2.154E2	4.258E2
CPU time for Alg. 2(b)	2.420E1	4.886E1	1.019E2	2.196E2	4.257E2
Alg. 2(a): l_{∞} Err.	3.141E-4	3.254E-4	3.177E-4	1.962E-4	4.993E-5
Alg. $2(a)$: l_2 Err.	1.779E-4	1.139E-4	7.382E-5	3.815E-5	9.267E-6
Alg. 2(b): l_{∞} Err.	1.864E-5	1.422E-5	1.780E-5	3.207E-5	5.570E-5
Alg. $2(b)$: l_2 Err.	1.465E-5	9.735E-6	8.503E-6	1.053E-5	1.715E-5

and the initial condition is

$$\phi(x, y, 0) = \exp(-(x^2 + y^2)/0.1).$$

The computational domain for the proposed methods is $[-1, 1]^2$, and the computational domain for the reference solution is $[-2, 2]^2$.

Figures 7, 8, and 9 show the plots of the numerical solutions by Algorithms 1 and 2, and the reference solutions.

 \bullet $\it Case~2$ (2-D vortices Bose–Einstein condensation [6, 12]): the potential is

$$v(x, y, t) = \frac{x^2 + y^2}{2} + W_s(t) \exp(-4((x - x_s(t))^2 + (y - y_s(t))^2)/V_s^2),$$

Table 4 1-D example, stability, and CPU time. l_{∞} error, l_2 error, and CPU time are recorded. For the proposed methods, $\Delta t = \Delta x/16$.

A /o	1 0	10.0	/	00 00)	
$\Delta x = \epsilon/8, \kappa = -1, C_p = 13; C_x = 5; \eta_x = \min(30\epsilon, 0.3)$					
ϵ	0.4	0.2	0.1	0.05	0.025
CPU time for Alg. 1	8.791	1.893E1	3.987E1	8.779E1	2.081E2
CPU time for Alg. 2(a)	8.479	1.964E1	3.553E1	8.002E1	1.657E2
CPU time for Alg. 2(b)	8.820	1.918E1	3.961E1	8.039E1	1.664E2
Alg. $2(a)$: l_{∞} Err.	4.349E-5	9.106E-6	5.653E-7	8.685E-8	7.020E-8
Alg. $2(a)$: l_2 Err.	3.148E-5	4.521E-6	1.670E-7	2.296E-8	1.457E-8
Alg. 2(b): l_{∞} Err.	2.318E-5	1.183E-6	1.120E-7	2.942E-8	2.481E-8
Alg. $2(b)$: l_2 Err.	2.388E-5	8.641E-6	6.531E-8	1.887E-8	2.032E-9
$\Delta x = \epsilon/8, \kappa = -1, C_p = 13; C_x = 2.5; \eta_x = 0.3$					
ϵ	0.4	0.2	0.1	0.05	0.025
CPU time for Alg. 1	1.019E1	1.924E1	4.009E1	8.660E1	2.303E2
CPU time for Alg. 2(a)	1.173E1	1.877E1	3.871E1	7.982E1	1.675E2
CPU time for Alg. 2(b)	1.019E1	1.933E1	3.857E1	7.903E1	1.670E2
Alg. 2(a): l_{∞} Err.	2.116E-5	6.023E-6	4.116E-7	9.375E-8	3.049E-8
Alg. $2(a)$: l_2 Err.	2.044E-5	3.282E-6	1.416E-7	3.160E-8	1.108E-8
Alg. 2(b): l_{∞} Err.	1.087E-6	2.336E-7	2.217E-8	5.687E-9	1.468E-8
Alg. $2(b)$: l_2 Err.	4.000E-7	1.746E-7	1.317E-8	3.873E-9	5.325E-9

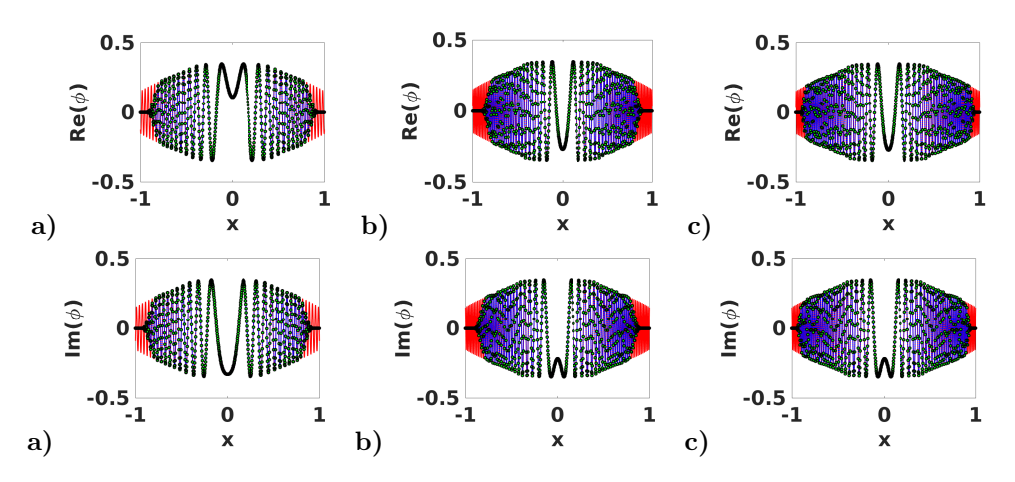


FIG. 3. 1-D example, plots of the numerical solutions ϕ at t=0.5. $\kappa=2$, $\Delta x=\epsilon/8$, $\Delta t=\Delta x/16$. Top: real part of ϕ ; Bottom: imaginary part of ϕ . Red line: refrerence solution; Blue dashed: Alg. 1; Green dots: Alg. 2(a); Black circle: Alg. 2(b). Column (a): $\epsilon=0.01, C_x=2.5, \eta_x=0.3;$ Column (b): $\epsilon=0.005, C_x=2.5, \eta_x=0.3;$ Column (c): $\epsilon=0.005, C_x=5, \eta_x=0.15.$

where $(x_s(t), y_s(t)) = (r_0 \cos(\omega_s t), r_0 \sin(\omega_s t))$, W_s increases linearly from 0 at t=0 to W_f at $t=\pi$, remains constant as W_f from $t=\pi$ to $t=4\pi$, decreases linearly to 0 at $t=5\pi$ from $t=4\pi$, and remains 0 after $t=5\pi$. We choose $W_f=\sqrt{2}, V_s=\sqrt{0.1}, r_0=2\sqrt{0.1}, \omega_s=1$. The initial condition is

$$\phi(x,y,0) = \sqrt{\max\left\{0, \mu - \frac{x^2 + y^2}{2}\right\}} \exp(-(x^2 + y^2)),$$

with μ a given constant.

The computational domain for the proposed methods is $[-2, 2]^2$, and the computational domain for the reference solution is $[-4, 4]^2$.

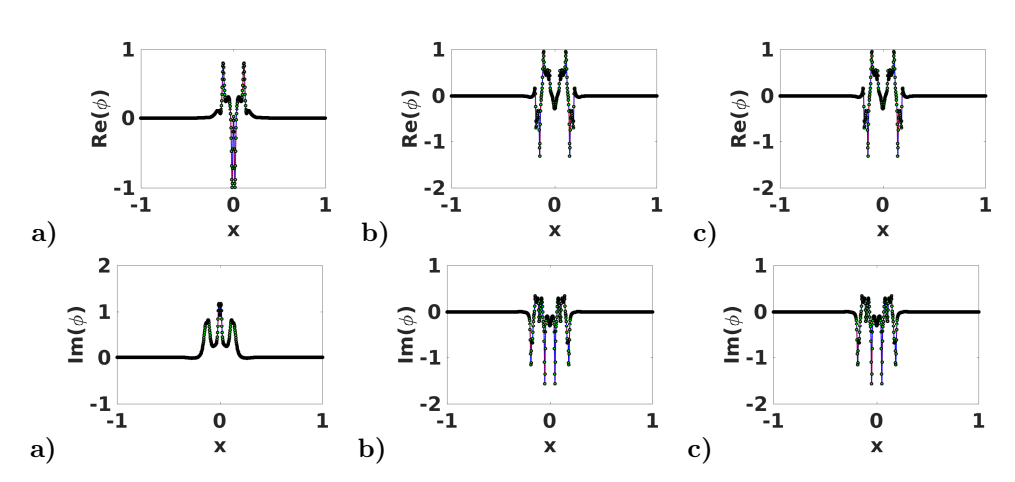


Fig. 4. 1-D example, plots of the numerical solutions ϕ at t=0.5. $\kappa=-1$, $\Delta x=\epsilon/8$, $\Delta t=\Delta x/16$. Top: real part of ϕ ; Bottom: imaginary part of ϕ . Red line: refrerence solution; Blue dashed: Alg. 1; Green dots: Alg. 2(a); Black circle: Alg. 2(b). Column (a): $\epsilon=0.01, C_x=2.5, \eta_x=0.3$; Column (b): $\epsilon=0.005, C_x=2.5, \eta_x=0.3$; Column (c): $\epsilon=0.005, C_x=5, \eta_x=0.15$.

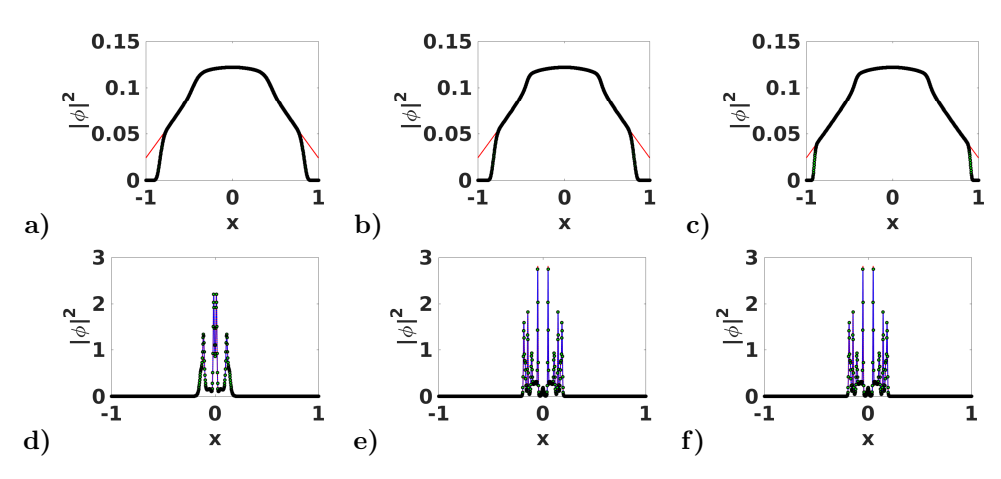


Fig. 5. 1-D example, plots of $|\phi|^2$ at t=0.5. $\Delta x=\epsilon/8$, $\Delta t=\Delta x/16$. Top: $\kappa=2$; Bottom: $\kappa=-1$. Red line: refrerence solution; Blue dashed: Alg. 1; Green dots: Alg. 2(a); Black circle: Alg. 2(b). (a-d): $\epsilon=0.01, C_x=2.5, \eta_x=0.3$; (b-e): $\epsilon=0.005, C_x=2.5, \eta_x=0.3$; (c-f): $\epsilon=0.005, C_x=5, \eta_x=0.15$.

Figures 10, 11, and 12 show the plots of the numerical solutions by Algorithms 1 and 2 and the reference solutions.

These figures verify the accuracy of the proposed methods.

3.1. Discussion of numerical experiments. From the numerical experiments, we note that

- for Algorithms 1 and 2, we can choose the mesh sizes as $\{\Delta x, \Delta y, \Delta z\} = O(\hbar)$ and $\Delta t = O(\{\Delta x, \Delta y, \Delta z\})$.
- For Algorithms 1 and 2, the order of accuracy is $O(\hbar + \{\Delta x, \Delta y, \Delta z\} + \Delta t)$, provided that the error due to the low-rank approximation with piecewise Chebyshev polynomial interpolation is not dominant.

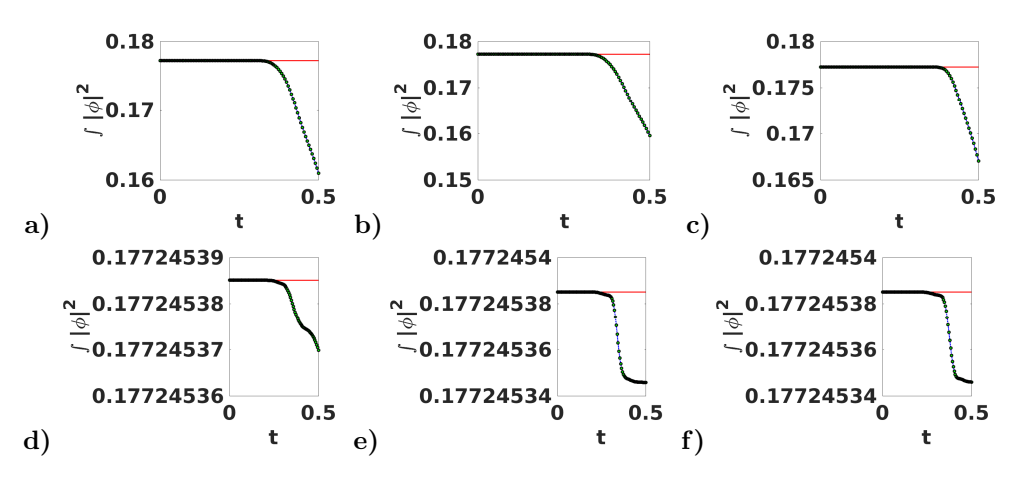


Fig. 6. 1-D example, plots of $\int |\phi|^2 dx$. $\Delta x = \epsilon/8$, $\Delta t = \Delta x/16$. Top: $\kappa = 2$; Bottom: $\kappa = -1$. Red line: refrerence solution; Blue dashed: Alg. 1; Green dots: Alg. 2(a); Black circle: Alg. 2(b). (a–d): $\epsilon = 0.01$, $C_x = 2.5$, $\eta_x = 0.3$; (b–e): $\epsilon = 0.005$, $C_x = 2.5$, $\eta_x = 0.3$; (c–f): $\epsilon = 0.005$, $C_x = 5$, $\sigma = 0.15$.

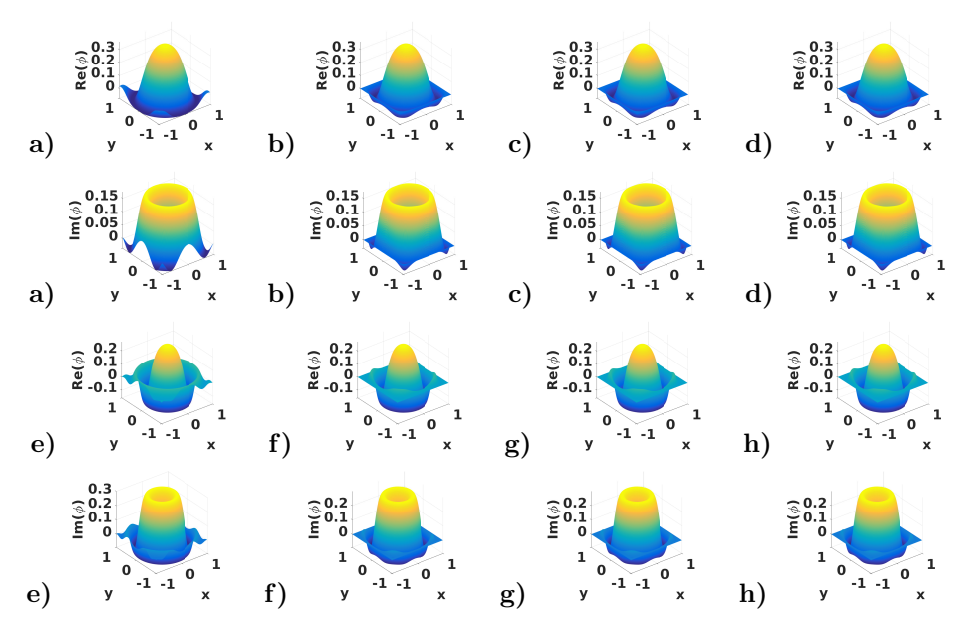


Fig. 7. 2-D example case 1: surface plots of the numerical solutions ϕ at t=0.8. (a–d) with $\epsilon=0.1$, (e–h) with $\epsilon=0.05$. $\kappa=1, \Delta x=\Delta y=\epsilon/4, \Delta t=\min\{\Delta x, \Delta y\}/8$. Top of (a–d) and (e–h): real part of ϕ , Bottom of (a–d) and (e–h): imaginary part of ϕ . From first column to fourth column: reference solution, Alg. 1, Alg. 2(a), and Alg. 2(b), respectively. For PMLs, $\eta_x=\eta_y=0.3$, $C_x=C_y=2.5$. For Algorithm 2(b), $C_p=C_q=13$.

• For Algorithm 1, if the width of the PMLs is independent of \hbar , the complexity is $O(N^2)$ due to the fact that direct summation is applied for computing the wavefunction in the PMLs; if the width of the PMLs is $O(\hbar)$, the complexity is $O(N \log N)$. For Algorithm 2, the complexity is $O(N \log N)$ for both choices of the PMLs.

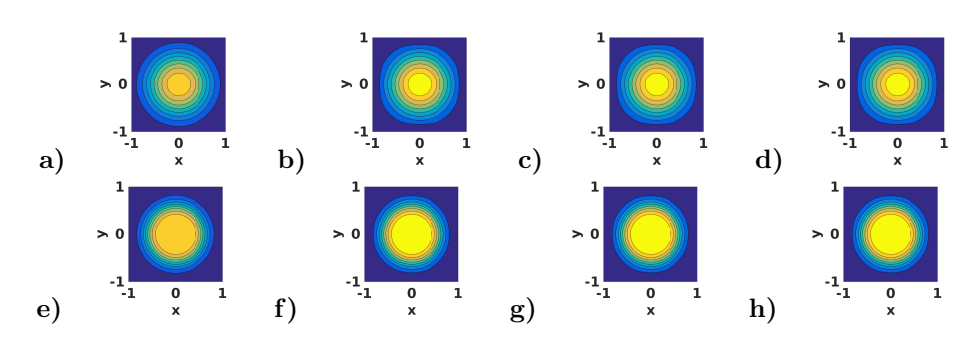


Fig. 8. 2-D example case 1: contour plots of $|\phi|^2$ at t=0.8. (a–d) with $\epsilon=0.1$, (e–h) with $\epsilon=0.05$. $\kappa=1, \Delta x=\Delta y=\epsilon/4, \Delta t=\min\{\Delta x, \Delta y\}/8$. From first column to fourth column: reference solution, Alg. 1, Alg. 2(a), and Alg. 2(b), respectively. For PMLs, $\eta_x=\eta_y=0.3, C_x=C_y=2.5$. For Algorithm 2(b), $C_p=C_q=13$.

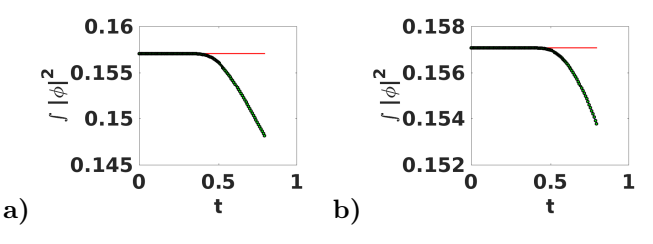


FIG. 9. 2-D example case 1: plots of $\int |\phi|^2 dx dy$. Red line: refrerence solution; Blue dashed: Alg. 1; Green dots: Alg. 2(a); Black circle: Alg. 2(b). (a) with $\epsilon = 0.1$, (b) with $\epsilon = 0.05$. $\kappa = 1, \Delta x = \Delta y = \epsilon/4, \Delta t = \min\{\Delta x, \Delta y\}/8$. For PMLs, $\eta_x = \eta_y = 0.3$, $C_x = C_y = 2.5$. For Algorithm 2(b), $C_p = C_q = 13$.

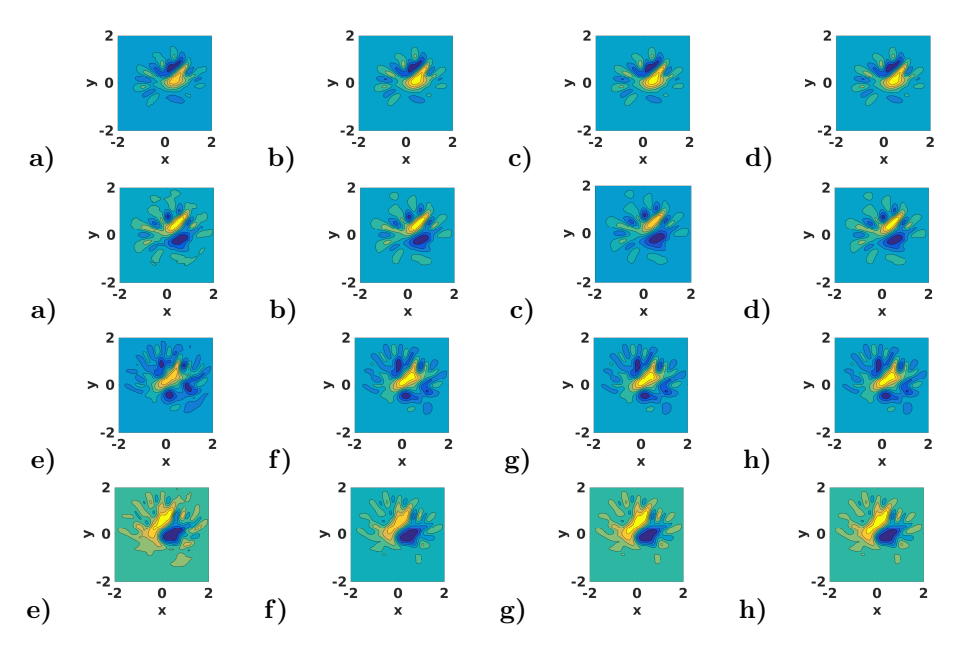


FIG. 10. 2-D example case 2: contour plots of the numerical solutions ϕ at $t=12\pi$ with $\epsilon=0.1$. (a–d) with $\mu=0.3$, (e–h) with $\mu=0.6$. $\kappa=1, \Delta x=\Delta y=\epsilon/4, \Delta t=\min\{\Delta x, \Delta y\}/8$. Top of (a–d) and (e–h): real part of ϕ , Bottom of (a–d) and (e–h): imaginary part of ϕ . From first column to fourth column: reference solution, Alg. 1, Alg. 2(a), and Alg. 2(b), respectively. For PMLs, $\eta_x=\eta_y=0.3, \ C_x=C_y=2.5$. For Algorithm 2(b), $C_p=C_q=13$.

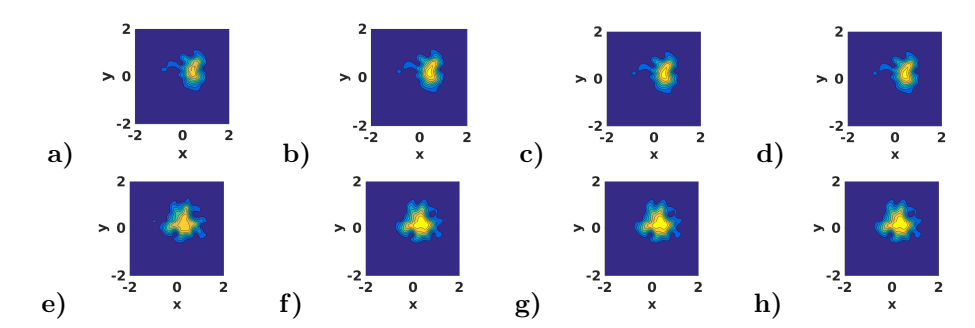


Fig. 11. 2-D example case 2: contour plots of $|\phi|^2$ at $t=12\pi$ with $\epsilon=0.1$. (a-d) with $\mu=0.3$, (e-h) with $\mu=0.6$. $\kappa=1, \Delta x=\Delta y=\epsilon/4, \Delta t=\min\{\Delta x, \Delta y\}/8$. From first column to fourth column: reference solution, Alg. 1, Alg. 2(a), and Alg. 2(b), respectively. For PMLs, $\eta_x=\eta_y=0.3, C_x=C_y=2.5$. For Algorithm 2(b), $C_p=C_q=13$.

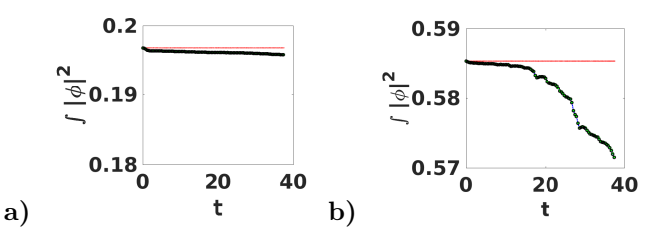


FIG. 12. 2-D example case 2: plots of $\int |\phi|^2 dx dy$ with $\epsilon = 0.1$. Red line: refrerence solution; Blue dashed: Alg. 1; Green dots: Alg. 2(a); Black circle: Alg. 2(b). (a) with $\mu = 0.3$, (b) with $\mu = 0.6$. $\kappa = 1, \Delta x = \Delta y = \epsilon/4, \Delta t = \min\{\Delta x, \Delta y\}/8$. For PMLs, $\eta_x = \eta_y = 0.3$, $C_x = C_y = 2.5$. For Algorithm 2(b), $C_p = C_q = 13$.

- Compared with Algorithm 1 that uses direct summation for points in the PMLs, Algorithm 2 with the low-rank approximation by piecewise Chebyshev polynomial interpolation is stable,
- 2-D examples on 2-D vortices Bose–Einstein condensation [6, 12] demonstrate that the proposed methods can be applied to solve real physical problems.
- 4. Conclusion. We present asymptotic methods, namely fast Huygens sweeping methods, for numerically solving the time-dependent Schrödinger equations with time-dependent potentials in the semi-classical regime. The PML techniques are applied to truncate the infinite domain to a bounded subdomain. The methods combine Huygens' principle and short-time WKBJ propagators, which results in integrals with the retarded Green's functions that approximated by the WKBJ expansion. Analytic approximations of the phase and amplitude terms in the WKBJ ansatz for the retarded Green's functions can be obtained via short-time Taylor expansions. For points in the PMLs, low-rank approximation by Chebyshev polynomial interpolation can be utilized to approximate the integrals such that the resulting integrals can be evaluated efficiently with FFT and the complexity is $O(N \log N)$ with N the number of points in the simulation. Numerical examples including time-dependent Gross-Pitaevskii equation for BEC are presented to demonstrate the proposed methods. The framework can be extended to include higher-order terms in the WKBJ ansatz and higher-order Taylor expansions for the phase and amplitude terms such that higher-order methods can be designed. The methods will be extended to study the time-dependent Kohn-Sham equations arising from electronic structure calculations, which will be reported in a future work.

REFERENCES

- X. Antoine, A. Arnold, C. Besse, M. Ehrhardt, and A. Schaedle, A review of transparent and artificial boundary conditions techniques for linear and nonlinear Schrödinger equations, Commun. Comput. Phys., 4 (2008), pp. 729–796.
- [2] X. Antoine, W. Bao, and C. Besse, Computational methods for the dynamics of the nonlinear Schrödinger/Gross-Pitaevskii equations, Comput. Phys. Commun., 184 (2013), pp. 2621–2633.
- [3] I. M. Babuška, F. Ihlenburg, T. Strouboulis, and S. K. Gangaraj, A posteriori error estimation for finite element solutions of helmholtz equation. Part II: Estimation of the pollution error, Int. J. Numer. Methods Engrg., 40 (1997), pp. 3883–3900.
- [4] I. M. BABUŠKA AND S. A. SAUTER, Is the pollution effect of the FEM avoidable for the Helmholtz equation considering high wave numbers?, SIAM Rev., 42 (2000), pp. 451–484.
- [5] B. BAKER AND E. T. COPSON, The mathematical theory of Huygens' principle, AMS Chelsea Publishing, Providence, RI, 1987.
- [6] W. BAO, D. JAKSCH, AND P. A. MARKOWICH, Numerical solution of the Gross-Pitaevskii equation for Bose-Einstein condensation, J. Comput. Phys., 187 (2003), pp. 318–342.
- [7] W. BAO, S. JIN, AND P. MARKOWICH, Numerical Study of Time-Splitting Spectral Discretizations of Nonlinear Schrödinger Equations in the Semiclassical Regimes, SIAM J. Sci. Comput., 25 (2003), pp. 27–64.
- W. BAO, S. JIN, AND P. A. MARKOWICH, On Time-Splitting Spectral Approximations for the Schrödinger Equation in the Semiclassical Regime, J. Comput. Phys., 175 (2002), pp. 487–524.
- [9] J.-P. Berenger, A perfectly matched layer for the absorption of electromagnetic waves, J. Comput. Phys., 114 (1994), pp. 185–200.
- [10] M. Brack and R. K. Bhaduri, Semiclassical Physics, Addison Wesley, Reading, MA, 1997.
- [11] E. CANDÉS, L. DEMANET, AND L. YING, A fast butterfly algorithm for the computation of Fourier integral operators, Multiscale Model. Sim., 7 (2009), pp. 1727–1750.
- [12] B. M. CARADOC-DAVIES, R. J. BALLAGH, AND K. BURNETT, Coherent dynamics of vortex formation in trapped Bose-Einstein condensates, Phys. Rev. Lett., 83 (1999), pp. 895–898.
- [13] P. CHAND AND J. HOEKSTRA, A review of the semi-classical WKB approximation and its usefulness in the study of quantum systems, in Proceedings of the IEEE Semiconductor Advances for Future Electronics, 2001, pp. 13–19.
- [14] J. W. COOLEY AND J. W. TUKEY, An algorithm for the machine calculation of complex Fourier series, Math. Comp., 19 (1965), pp. 297–301.
- [15] L. Demanet, M. Ferrara, N. Maxwell, J. Poulson, and L. Ying, A butterfly algorithm for synthetic aperture radar imaging, SIAM J. Imaging Sci., 5 (2012), pp. 203–243.
- [16] B. ENGQUIST AND O. RUNBORG, Computational high frequency wave propagation, Acta Numerica, 12 (2003), pp. 181–266.
- [17] S. FOMEL, L. YING, AND X. SONG, Seismic wave extrapolation using lowrank symbol approximation, Geophys. Prospect., 61 (2013), pp. 526-536.
- [18] D. FUJIWARA, A construction of the fundamental solution for the Schrödinger equations, Proc. Japan Acad. Ser. A Math. Sci., 55 (1979), pp. 10–14.
- [19] S. Jin, P. Markowich, and C. Sparber, Mathematical and computational methods for semiclassical Schrödinger equations, Acta Numerica, 20 (2011), p. 121–209.
- [20] J. B. Keller, Semiclassical mechanics, SIAM Rev., 27 (1985), pp. 485–504.
- [21] H. KITADA AND H. KUMANO-GO, A family of Fourier integral operators and the fundamental solution for a Schrödinger equation, Osaka J. Math., 18 (1981), pp. 291–360.
- [22] S. LEUNG, J. QIAN, AND S. SERNA, Fast Huygens sweeping methods for Schrödinger equations in the semi-classical regime, Methods Appl. Anal., 21 (2014), pp. 31–66.
- [23] S. Luo, J. Qian, and R. Burridge, Fast Huygens sweeping methods for Helmholtz equations in inhomogeneous media in the high frequency regime, J. Comput. Phys., 270 (2014), pp. 378–401.
- [24] S. Luo, J. Qian, and R. Burridge, High-order factorization based high-order hybrid fast sweeping methods for point-source Eikonal equations, SIAM J. Numer. Anal., 52 (2014), pp. 23–44.
- [25] A. MARTINEZ, An introduction to semiclassical and microlocal analysis, Springer, New York, 2002.
- [26] V. P. MASLOV AND M. V. FEDORIUK, Semi-classical approximation in quantum mechanics, D. Reidel Publishing Company, Boston, 1981.

- [27] J. Qian, W. Lu, L. Yuan, S. Luo, and R. Burridge, Eulerian geometrical optics and fast Huygens sweeping methods for three-dimensional time-harmonic high-frequency Maxwell's equations in inhomogeneous media, Multiscale Model. Sim., 14 (2016), pp. 595-636.
- [28] J. QIAN, S. Luo, and R. Burridge, Fast Huygens sweeping methods for multi-arrival Green's functions of Helmholtz equations in the high frequency regime, Geophysics, 80 (2015), pp. T91-T100.
- [29] L. S. Schulman, Techniques and Applications of Path Integration, Wiley, New York, 1981.
- [30] G. STRANG, On the Construction and Comparison of Difference Schemes, SIAM J. Numer. Anal., 5 (1968), pp. 506–517.
- [31] A. ZAGOSKIN, Quantum Theory of Many-Body Systems: Techniques and Applications, 2nd ed., Springer, New York, 2014.
- [32] C. Zheng, A perfectly matched layer approach to the nonlinear Schrödinger wave equations, J. Comput. Phys., 227 (2007), pp. 537–556.